IJEMD-M, 4 (1) (2026) https://doi.org/ 10.54938/ijemdm.2026.04.1.593
International Journal of Emerging Multidisciplinaries:
Mathematics
Research Paper
Journal Homepage: www.ojs.ijemd.com
ISSN (print): 2790-1998

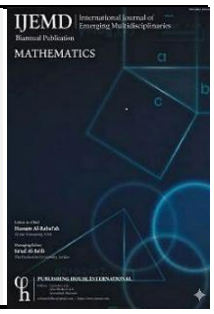

Computational Effects of Heat Transfer in Ostwald–de Waele Fluid with a Nonlinearly Stretching Cylinder

Walija Gul [1], Zaffer Elahi [1], Tahir Naseem *[2]

1. Department of Mathematical Sciences, University of Engineering and Technology, Taxila-47050, Pakistan
2. Pak-Austria Fachhochschule Institute of Applied Sciences and Technology (PAF-IAST), 22600, Pakistan

Abstract

This study explores the steady flow and heat transfer of an Ostwald–de Waele (power-law) fluid across a cylinder with nonlinear stretching, encompassing convective heating, nonlinear radiation, Joule heating, and a variable magnetic field. The governing boundary-value problem is worked out using MATLAB's BVP4C collocation scheme and justified against existing literature. Three fluid types pseudoplastic, Newtonian, and dilatant fluids are observed to assess the influence of shear-dependent viscosity. The findings show that stretching nonlinearity plays a primary role in transport phenomena: nonlinear stretching (m = 2) consistently leads to higher skin-friction coefficients and larger Nusselt numbers than linear stretching, indicating strengthened near-wall gradients. Thermal responses depend on the controlling factor Ec, M, κ, ϕ, and R produce higher temperatures under linear stretching, whereas Pr reduces temperature more effectively under nonlinear stretching. Curvature enhances heat removal for all fluids, while magnetic damping suppresses heat transfer. These findings offer guidance for polymer extrusion and thermal processing of cylindrical materials.

Keywords: Power law fluid; Nonlinear-Stretching; Horizontal Cylinder; Joule Heating; Variable Magnetic field; Convective condition

Email Addresses: 22-MS-MTH-3@students.uettaxila.edu.pk (Walija Gul) , zaffer.elahi@uettaxila.edu.pk (Zafer Elahi) , tahir.naseem@paf-iast.edu.pk (Tahir Naseem)

1 Nomenclature

u	Velocity component along t directions
w	Velocity component along s directions
m	Stretching exponent
σ^*	Stephen Boltzmann constant
k_o	Mean absorption constant
$B(s)$	Variable Magnetic field
η	Similarity variable
ζ	Stream function
α	Thermal diffusivity of fluid
R_o	Radius of cylinder
Φ	Surface Convection parameter
γ	Slip parameter
q_{rad}	Non-linear radioactive heat flux
h	Convective thermal transport coefficient

2 Introduction

Non-Newtonian fluids, particularly those described by the Ostwald–de Waele (power-law) model, continue to attract significant interest due to their importance in polymer processing, biochemical materials, coating technologies, and energy systems. Their shear-dependent viscosity enables accurate modeling of pseudoplastic and dilatant behaviours, which strongly influence momentum and heat transport. Recent works highlight the renewed relevance of power-law fluids in modern engineering applications, including polymer extrusion, biofluids, and manufacturing of thin films [1], [2]. Flow over stretching surfaces remains one of the most studied configurations because of its direct applications in processes such as hot rolling, wire coating, textile manufacturing, and sheet extrusion. Recent contributions investigating non-Newtonian or power-law fluids over stretching sheets include [3], who studied thermally radiative power-law flow [4], who examined heat transfer in power-law fluids with nonlinear stretching; and [5], who analyzed entropy generation in power-law boundary layers. These studies emphasize that stretching rates significantly influence boundary-layer thickness and thermal gradients. Compared to stretching flat sheets, flows driven by stretching cylinders have received relatively less attention despite their direct relevance in fibre formation, cable coating, cylindrical extrusion, and biomedical devices. Recent studies include [6] on momentum transfer over a linearly stretching cylinder , [7] analyzing mass transfer in axisymmetric stretching cylinders , and [8] who examined power-law flow with magnetic effects over a stretching cylinder. These works demonstrate that geometry introduces curvature-driven effects not present in planar surfaces.

However, only a few recent studies have considered nonlinear stretching cylinders, even though nonlinear stretching better represents practical extrusion and manufacturing processes. Notable contributions include [9] who explored nonlinear stretching with thermal radiation, and [10] who incorporated variable

thermophysical properties. Despite these advancements, power-law fluids subjected to nonlinear stretching in cylindrical geometries remain insufficiently investigated.

Convective boundary conditions (CBCs) are essential in modelling realistic thermal systems such as heat exchangers, nuclear reactors, porous materials, micro-devices, and energy storage units. Recent developments include [11] who analysed convective heating on stretching surfaces, [12] who examined convective cooling in nonnewtonian sheet flows, and [13] who explored convective MHD non-Newtonian flow with viscous dissipation. These works show that convective boundaries significantly alter temperature distributions and Nusselt numbers.

Despite substantial progress, no study has simultaneously investigated power-law rheology, nonlinear stretching velocity, cylindrical geometry, magnetic field variation, viscous dissipation, Joule heating, and thermal radiation under convective heating conditions. The present work fills this gap by analysing the steady axisymmetric flow and heat transfer of an Ostwald–de Waele fluid over a nonlinearly stretching cylinder incorporating all these physical effects. Similarity transformations reduce the governing PDEs to nonlinear ODEs, which are solved numerically to characterize the influence of the power-law index, stretching parameter, curvature factor, magnetic field, and thermal parameters on fluid motion, temperature distribution, skin friction, and heat transfer rate.

3 Problem Formulation

Consider a steady, incompressible, two-dimensional boundary layer flow of a viscous fluid obeying the power-law model incorporating the effect of a variable magnetic field B. The magnetic field strength is defined as $B = B_o s^{\frac{(m-1)}{2}}$ where B_o is a constant. The s-axis of fluid flow aligns with the axial direction of the cylinder, as illustrated in Figure below, while the t-axis is perpendicular to it.

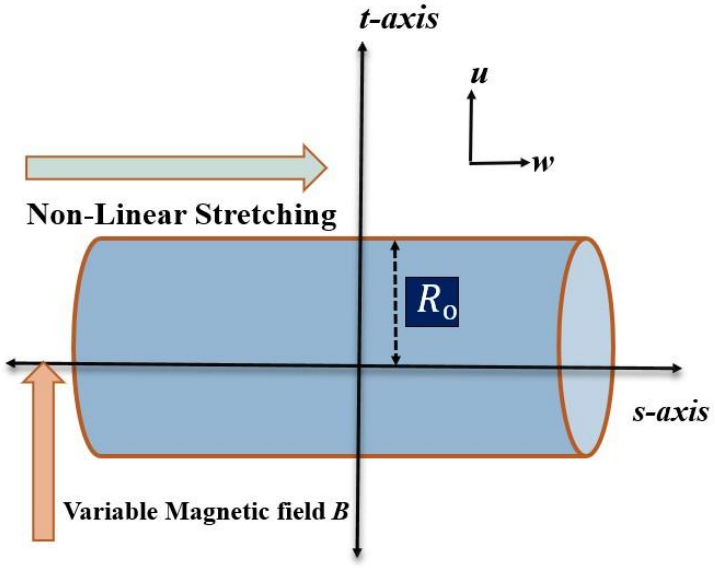

Figure 1: Schematic of the Stretching Cylinder Geometry

3.1 Fluid Flow Modeling

The continuous stretched cylinder is considered to have a nonlinear velocity of the type $U(s) = as^m$. By executing boundary-layer approximation, the fundamental equations are

$$t\ u_t + u + t\ w_s = 0, \quad (1)$$

$$u\ w_t + w\ w_s = -\frac{k}{\rho}\frac{1}{t}\left[(-w_t)^n + n(-w_t)^{n-1}w_{tt}\right] - \frac{\sigma}{\rho}wB^2, \quad (2)$$

The relevant boundary conditions of velocity, according to [14]

$$u = 0,\ w = as^m + \varepsilon|w_t|^{n-1}w_t, \quad at \qquad t = R_o$$

$$u = 0,\ w = 0, \qquad as \qquad t \to \infty. \quad (3)$$

Eqn. (1), get fulfilled through the inclusion of the stream function ζ, resulting in

$$u = -\frac{1}{t}\zeta_s, \qquad w = \frac{1}{t}\zeta_t$$

Following [15, 16], we define η and, ζ as

$$\eta = \frac{t^2 - R_o^2}{2R_o s}Re^{\frac{1}{n+1}}, \qquad \zeta = \frac{aRs^{m+1}}{Re^{\frac{1}{n+1}}}h(\eta) \quad (4)$$

Using Eqn. (4), the momentum Eqn. (2) becomes

$$(n+1)\ \kappa\ (1+2\eta\kappa)^{\frac{n-1}{2}}(-h'')^n - h\ h''\left(\frac{m\ (2\ n-1)+1}{n+1}\right) - n\ (1+2\eta\kappa)^{\frac{n+1}{2}}\ h'''(-h'')^{n-1}$$

$$+(m\ h' + M)\ h' = 0 \quad (5)$$

together with boundary conditions

$$At\ \eta = 0,\ h(\eta) = 0,\ h'(\eta) = 1 - \gamma(-h''(\eta))^n,\ and\ h'(\eta) \to 0,\ as\ \eta \to \infty, \quad (6)$$

where,

$Re = \frac{as^{m+n}\rho}{k}$ shows Reynolds parameter, $\kappa = \frac{s}{R_o}Re^{\frac{-1}{n+1}}$ is the curvature parameter,

$M = \frac{\sigma B_o^2}{\rho a}$ is the magnetic parameter, $\gamma = \frac{U^{n-1}\varepsilon}{s^n}Re^{\frac{n}{n+1}}$ shows slip parameter.

3.1.1 Skin friction

The expression for the Surface shear stress is given as

$$C_f = \frac{2\tau_w}{\rho(as)^m} \qquad where \qquad \tau_w = \ k\ [(w_t)^n]_{t=R_o}. \quad (7)$$

The non-dimensional form of skin friction (wall shear stress) is given as

$$C_f\frac{1}{2}Re^{\frac{1}{n+1}} = -\left[-h''(0)\right]^n \quad (8)$$

3.2 Heat Transfer Modeling

The fluid's ambient temperature is T_∞, and the temperature at the wall of the cylinder is T_w, defined as $T_w = T_\infty + As^m$, where $T_w > T_\infty$. The heat flow problem for the stretching cylinder to the fluid is governed by

$$u\ T_t + w\ T_s = \alpha(-w_t)^{n+1} - \frac{k_1}{\rho C_p}\left(T_{tt} + \frac{1}{t}T_t\right) - \frac{(q_{rad})_t}{\rho C_p} + \frac{\sigma}{\rho C_p}w^2B^2, \tag{9}$$

where $\alpha = \frac{k}{\rho C_p}$ is thermal diffusivity and $k_1 = k_* |T_t|^{n-1}$ is constant thermal conductivity.
By applying the Rosseland approximation [17], non-linear radioactive heat flux is defined as

$$q_{rad} = -\frac{4\sigma^*}{3k_o}T_t^4, \tag{10}$$

By following Raptis [14], eliminate higher-order terms and expanding T_4 in a Taylor series, we have

$$T^4 \approx 4T_\infty^3 T - 3T_\infty^4.$$

when employing the heat flux q_{rad} term, *i.e*, Eqn. (10) in Eqn. (9), we get

$$u\ T_t + w\ T_s = \alpha(-w_t)^{n+1} - \frac{k_1}{\rho C_p}\left(T_{tt} + \frac{1}{t}T_t\right) + \frac{1}{\rho C_p}\frac{16\sigma^* T_\infty^3}{3k_o}\ T_{tt} + \frac{\sigma}{\rho C_p}w^2B^2, \tag{11}$$

Where α is thermal diffusivity. To complete the problem, the boundary conditions of temperature are

$$-T_t = \frac{h}{k}(T_w - T), \quad at \quad t = R_o, \quad and \quad T \to T_\infty, \quad as \quad t \to \infty. \tag{12}$$

Employing similarity transformations, as

$$T - T_\infty = (T_w - T_\infty)\,\theta(\eta) \tag{13}$$

In consideration of Eqn. (13), Eqn. (11) leads to

$$E_c\ (-h'')^{n+1}(1+2\eta\kappa)^{\frac{n+1}{2}} - \left(\frac{m(2\ n-1)+1}{n+1}\right)\theta' h + \frac{2\ \kappa}{Pr}(1+2\eta\kappa)^{\frac{n-1}{2}}(-\theta')^n\left(1+\frac{2}{3}R\right)$$

$$+m\ \theta\ h' + M\ E_c\ h'^2 - \frac{1}{Pr}\ (1+2\eta\kappa)^{\frac{n+1}{2}}\ \theta''(-\theta')^{n-1}\left(1+\frac{4}{3}R\right) = 0, \tag{14}$$

along with boundary conditions

$$At\ \eta = 0, \quad \theta'(\eta) + \Phi - \theta(\eta)\Phi = 0, \quad and \quad \theta(\eta) \to 0, \quad as\ \eta \to \infty, \tag{15}$$

where $Pr = C_p\frac{k}{k_1}\left(\frac{a}{A}\right)^{n+1}$ shows Prandtl parameter, $\Phi = \frac{-hs}{kRe^{\frac{1}{n+1}}}$ is the convection parameter, $E_c = \frac{U^2}{C_p(T_w - T_\infty)}$ shows Eckert parameter, $R = \frac{4T_\infty^3\sigma^*}{k_o k_1}$ shows radiation variable.

3.2.1 Nusselt number

An expression for the Nusselt parameter (temperature gradient) is presented as

$$N_u = \frac{s\ q_w}{k\ (T_w - T_\infty)} \qquad when \qquad at \qquad t = R_o, \qquad q_w = -k\ (T_t) \qquad . \tag{16}$$

Thus, the non-dimensional form of Eqn. (16) can be obtained

$$\frac{N_u}{Re^{\frac{1}{n+1}}} = -\theta'(0) \qquad . \tag{17}$$

4 Numerical Scheme

The numerical results of reduced boundary value problems, which are nonlinear in nature, are computed in the software MATLAB using the algorithm BVP4C. When compared to other approaches like NDSOLVE, HAM, and several other numerical techniques, the BVP4C solver is a more efficient solver. In order to apply the BVP4C solver, the initial guesses must meet the boundary limits. By exchanging the characterised variables, the coupled ODEs (5, 13) and their corresponding boundary conditions (6, 14) become a system of first-order equations. Letting

$$\lambda_1 = h, \tag{18}$$

$$= \quad ' \tag{19}$$

$$\lambda_2 \quad h\ , \quad = \quad '' \tag{20}$$

$$\lambda_3 \quad h\ , \quad \lambda_3' = \quad ''' \quad h\ , \tag{21}$$

$$\lambda_4 = \theta, \tag{22}$$

$$\lambda_5 = \theta', \tag{23}$$

$$\lambda_5' = \theta'', \tag{24}$$

where,

$$\lambda_3' = \frac{(n+1)\ \kappa\ (1+2\eta\kappa)^{\frac{n-1}{2}}(-\lambda_3)^n + M\ \lambda_2 + m\ \lambda_2^2 - \lambda_1\lambda_3\left(\frac{m\ (2n-1)+1}{n+1}\right)}{n\ (1+2\eta\kappa)^{\frac{n+1}{2}}(-\lambda_3)^{n-1}},$$

$$\lambda_5' = \frac{1}{(1+2\eta\kappa)^{\frac{n+1}{2}}(-\lambda_5)^{n-1}(1+\frac{4}{3}R)}\Big[m\ Pr\ \lambda_2\lambda_4 - E_c\ Pr\ (-\lambda_3)^{n+1}(1+2\eta\kappa)^{\frac{n+1}{2}}$$

$$+2\ \kappa(1+2\eta\kappa)^{\frac{n-1}{2}}(-\lambda_5)^n\left(1+\frac{2}{3}R\right) - \left(\frac{m\ (2n-1)+1}{n+1}\right) Pr\ \lambda_1\lambda_5 - M\ E_c\ Pr\ \lambda_2^2\Big], \tag{25}$$

under conditions $\lambda_1(0) = 0$, $\lambda_2(0) = 1 - \gamma(-\lambda_3(0))^n$, $\lambda_5(0) = -\Phi(1 - \lambda_4(0))$, $\lambda_2(\infty) = 0$, $\lambda_4(\infty) = 0$. (26)

4.1 Validity of Numerical Scheme

This section presents numerical findings for relevant quantities obtained by applying the BVP4C technique via MATLAB. The validity and efficiency of the BVP4C approach are shown in Table (1).

Table 1: Validation of $-\theta'(0)$ values at $Ec = R = \gamma = \kappa = 0$

Φ	Aziz [18]			Ishak [19]			PresentOutcomes		
	Pr=0.1	Pr=0.72	Pr=10	Pr=0.1	Pr=0.72	Pr=10	Pr=0.1	Pr=0.72	Pr=10
0.05	0.0373	0.0428	0.0468	0.0368	0.0427	0.0467	0.0372	0.0428	0.0484
0.1	0.0594	0.0747	0.0879	0.0583	0.0747	0.0879	0.0593	0.0748	0.0940
0.2	0.0848	0.1193	0.1569	0.0823	0.1192	0.1569	0.0843	0.1197	0.1776
0.4	0.1076	0.1700	0.2582	0.1037	0.1699	0.2581	0.1069	0.1708	0.3194

Table 2 verifies the results by calculating numerical values of $f''(0)$ and comparing them to prior research under certain limitations. Table 2 compares the value of $f''(0)$ to those of Mishra *et al.* [20], Abel *et al.* [21], and Anderson [22] for $M = 0$, indicating the suggested scheme's validity, accuracy, and efficancy. Furthermore, the provided findings illustrate the benefit of the BVP4C method.

Table 2: Validation of $f''(0)$ when M=0

n	Mishra *et al.* [20]	Abel *et al.*[21]	Anderson[22]	present results
0.2	1.9444	1.9436	1.9287	1.9509
0.5	1.1671	1.1677	1.1605	1.1705
1	1.0000	1.0000	1.0000	1.0000
1.2	0.9873	0.9873	0.9874	0.9873

5 Observations and Insights

Graphical simulations were performed across the heat transport profile for varying magnetic numbers M, Eckert numbers Ec, nonlinear stretching exponents m, curvature parameters κ, Biot parameters Φ, and Prandtl parameters denoted as Pr. The ultimate aim of the current investigation is to explore the impact of these variables on heat transport.

Figure 2 illustrates the diversity of the Eckert number on thermal transport for pseudoplastic, Newtonian, and dilatant fluids under linear and nonlinear stretching conditions. The temperature rises with increasing Ec in all cases because higher Eckert number represents stronger viscous dissipation, whereby mechanical energy is irreversibly converted into thermal energy and directly heats the fluid. The magnitude of this heating effect depends on the rheology of the fluid. For pseudoplastic fluids ($n < 1$), the effective viscosity decreases with shear, allowing the dissipation-generated heat to diffuse more quickly, producing a relatively steeper rise in temperature. Newtonian fluids ($n = 1$) displays a moderate outcome since their

viscosity is constant, while dilatant fluids ($n > 1$) shows the highest thermal resistance due to shear-thickening behaviour, resulting in comparatively flatter temperature

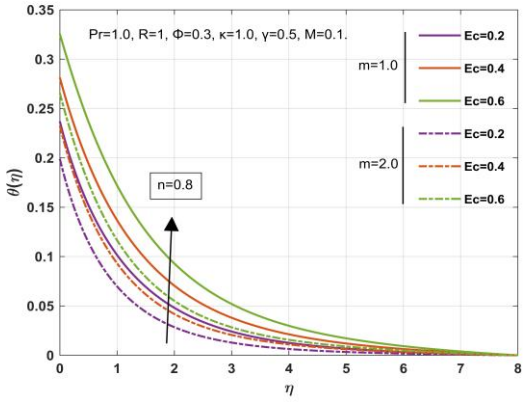

(a) Eckert effect on Pseudoplastic fluid

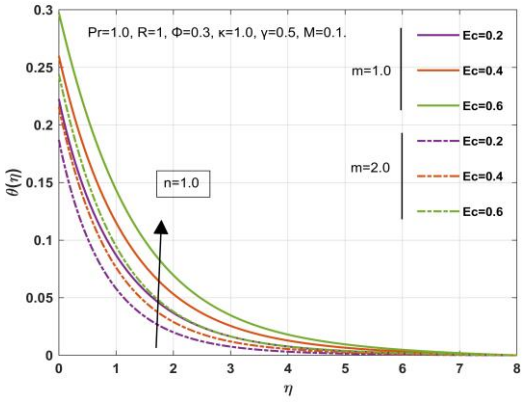

(b) Eckert effect on Newtonian fluid

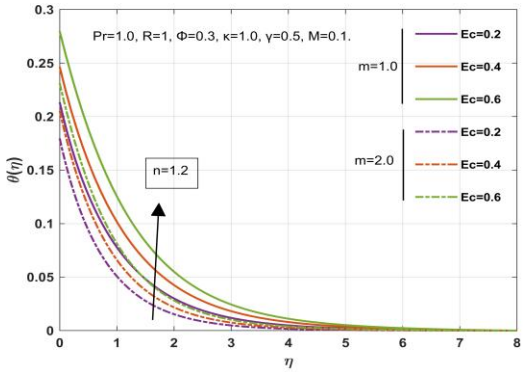

(c) Eckert effect on Dilatant Fluid

Figure 2: (a-c) Diversity of E_c parameter on thermal transport

profiles. Furthermore, linear stretching ($m = 1$) consistently leads to higher temperature levels than nonlinear stretching ($m = 2$). This happens because linear stretching generates a uniform and stronger shear field near the surface, which intensifies viscous dissipation more effectively, whereas nonlinear stretching delivers shear more gradually, weakening the heat generation. Mainly, Figure 2 shows that the combined effects of viscous dissipation, stretching intensity, and shear-dependent viscosity govern the different thermal responses observed across the three fluid types.

Figure 3 depicts the effect of the magnetic parameter M on the temperature field for pseudoplastic, Newtonian, and dilatant fluids under linear and nonlinear stretching. Increasing M strengthens the Lorentz force, which suppresses fluid motion and reduces convective heat removal, thereby producing higher temperature profiles. The extent of this magnetic heating varies with rheology: pseudoplastic fluids show a milder rise due to shear-thinning behaviour, Newtonian fluids display a moderate increase, while dilatant fluids exhibit the strongest thermal buildup because of their shear-thickening resistance. Additionally, lin-

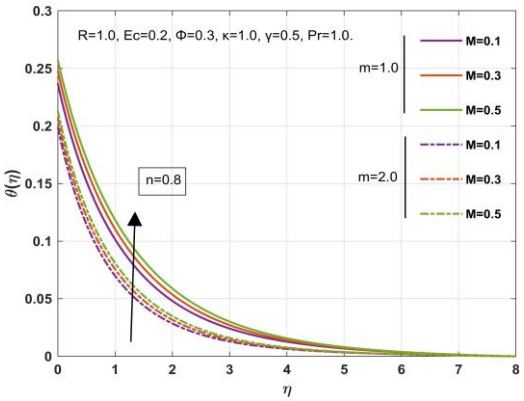

(a) Magnetic effect on Pseudoplastic fluid

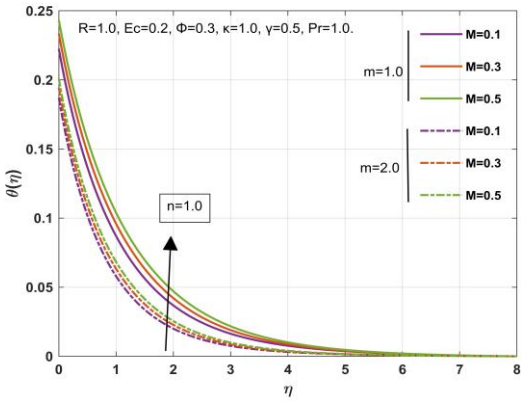

(b) Magnetic effect on Newtonian fluid

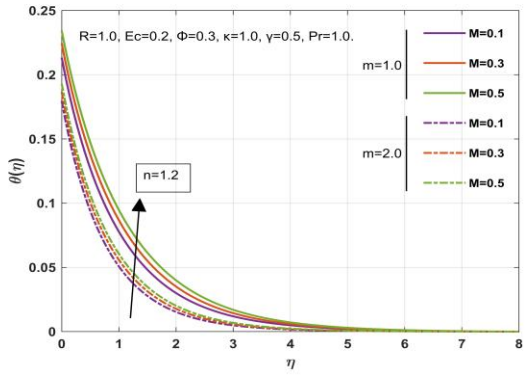

(c) Magnetic effect on Dilatant Fluid

Figure 3: (a-c) Diversity of *M* parameter on thermal transport

ear stretching ($m = 1$) leads to consistently higher temperatures than nonlinear stretching ($m = 2$), as the uniform shear produced under linear stretching engages more effectively with the Lorentz force, enhancing the magnetic damping. Overall, the combined action of magnetic resistance and shear distribution regulates the observed temperature trends along the three fluid types.

Figure 4 depicts the impact of the curvature parameter κ on the temperature distribution for pseudoplastic ($n < 1$), Newtonian ($n = 1$), and dilatant ($n > 1$) fluids under both stretching modes. Increasing κ corresponds to a stronger geometric curvature (smaller cylinder radius), which intensifies radial convection and compresses the thermal boundary layer. As a result, the temperature profile becomes thinner at larger curvature values, indicating improved heat removal from the surface. The sensitivity to curvature relies strongly on the rheology. Pseudoplastic fluids (shear-thinning) show the most articulated reduction in temperature due to their lower effective viscosity, which enables curvature driven convection to dominate. Newtonian fluids show moderate behaviour, while dilatant fluids (shear-thickening) shows the weakest impacts of κ because the increased viscosity opposes curvature-induced deformation. For all fluid types, linear stretching ($m = 1$) exhibits a stronger curvature effect than nonlinear stretching ($m = 2$).

The higher strain rate in the $m = 1$ case intensifies near-wall gradients, making the thermal boundary layer more adaptive to geometric curvature.

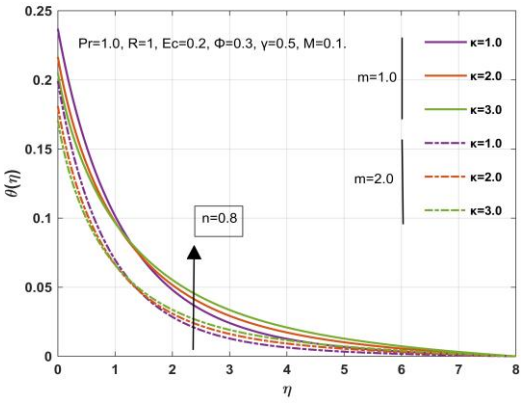

(a) Curvature effect on Pseudoplastic fluid

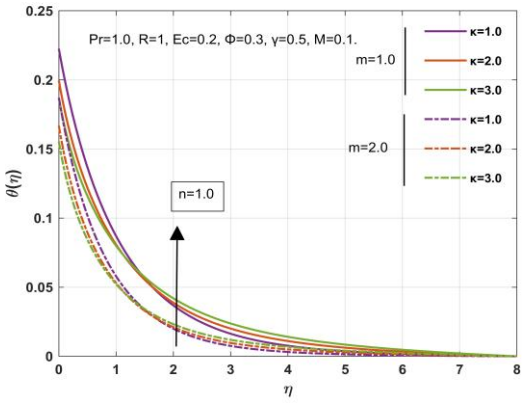

(b) Curvature effect on Newtonian fluid

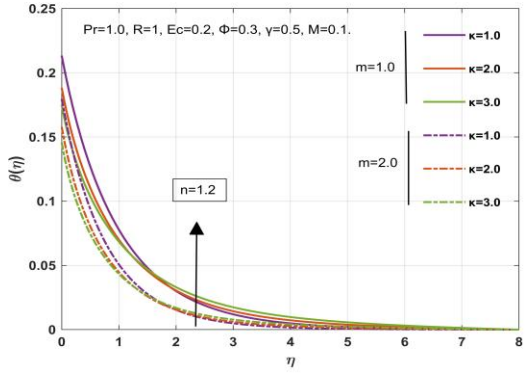

(c) Curvature effect on Dilatant Fluid

Figure 4: (a-c) Diversity of κ parameter on thermal transport

Figure 5 shows the impacts of the Prandtl number Pr on the temperature fields for pseudoplastic, Newtonian, and dilatant fluids under linear and nonlinear stretching. Since a higher Pr decrease in thermal diffusivity makes the fluid less capable of spreading heat, causing the thermal boundary layer to shrink and the temperature to drop more swiftly. This effect appears in all three fluids, though its strength changes with rheology: pseudoplastic fluids, being shear-thinning, show the most pronounced reduction; Newtonian fluids display a moderate decline; and dilatant fluids preserves more heat due to their shear-thickening nature. In contrast to the behaviour seen for Eckert number, magnetic parameter, or curvature, the influence of Pr is stronger in the nonlinear stretching case ($m = 2$). This happens because nonlinear stretching produces a weaker near-wall shear environment, making the reduced thermal diffusivity at higher Pr. As a result, the temperature decreases more rapidly for nonlinear stretching than for linear stretching, where the stronger, uniform shear partially offsets the diffusivity-controlled thinning of the

thermal layer. Thus, the interaction between thermal diffusivity and the shear distribution created by each stretching mode explains the stronger *Pr* dependence in the nonlinear case.

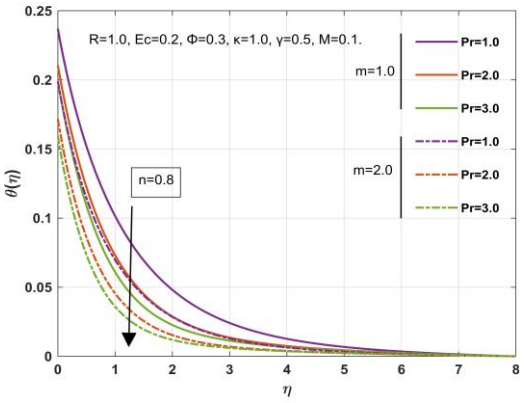

(a) Prandtl effect on Pseudoplastic fluid

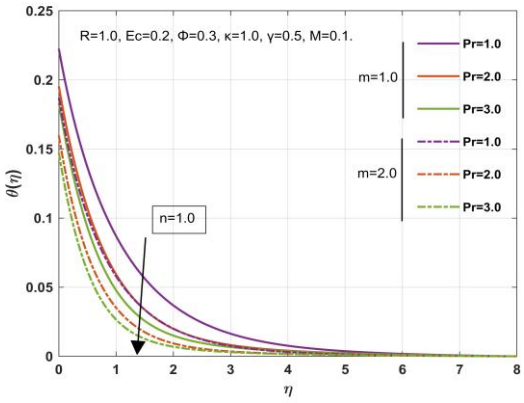

(b) Prandtl effect on Newtonian fluid

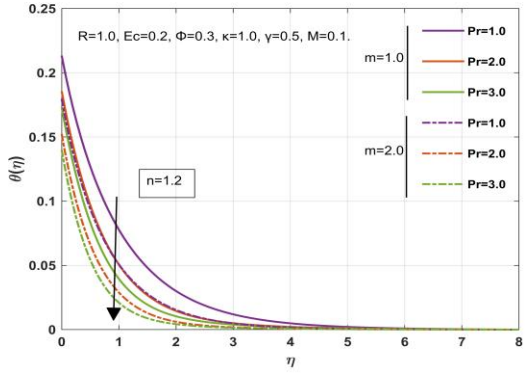

(c) Prandtl effect on Dilatant Fluid

Figure 5: (a-c) Diversity of *Pr* parameter on thermal transport

Figure 6 shows that intensifying the Biot number ϕ raises the temperature for pseudoplastic, Newtonian, and dilatant fluids. A larger ϕ improves surface convection, allowing more heat to enter the fluid from the wall and generating higher temperature profiles. The magnitude of this growth depends on rheology: pseudoplastic fluids deliver the added heat more readily, Newtonian fluids show a moderate increase, while dilatant fluids secure heat closer to the surface due to shear thickening. Corresponding to the Eckert number, linear stretching (m = 1) generates a stronger thermal response than nonlinear stretching (m = 2) because the uniform shear in the linear case intensifies the transfer of wall-generated heat into the flow.

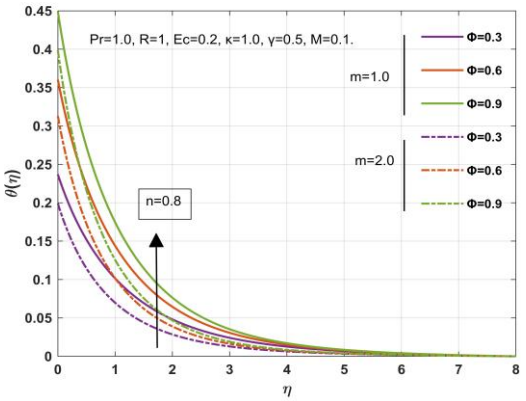

(a) Convection effect on Pseudoplastic fluid

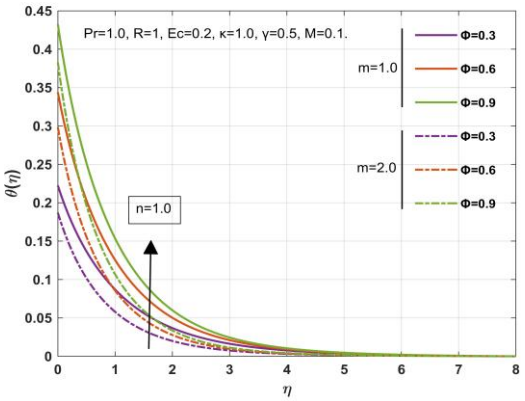

(b) Convection effect on Newtonian fluid

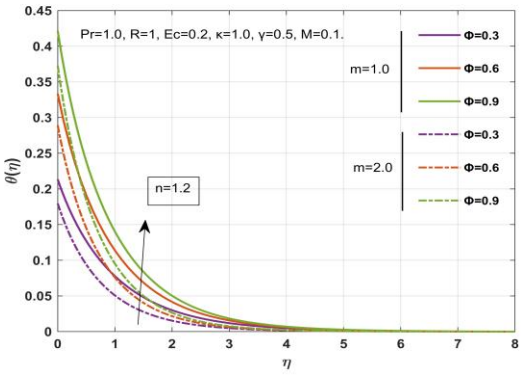

(c) Convection effect on Dilatant Fluid

Figure 6: (a-c) Diversity of ϕ parameter on thermal transport

Figure 7 shows that increasing the radiation parameter R boosts the temperature for pseudoplastic, Newtonian, and dilatant fluids. A larger R enhances radiative heat flux, adding thermal energy directly into the fluid and thickening the thermal boundary layer. Pseudoplastic fluids show a sharper rise due to easier heat diffusion, Newtonian fluids respond moderately, and dilatant fluids display a comparatively smaller increase. As with the Biot and Eckert numbers, linear stretching ($m = 1$) produces a stronger thermal effect than nonlinear stretching ($m = 2$), because the uniform shear in the linear case promotes more efficient absorption and redistribution of radiative heat within the boundary layer.

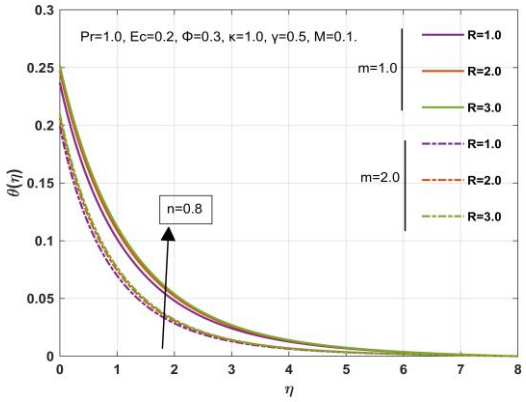

(a) Radiation effect on Pseudoplastic fluid

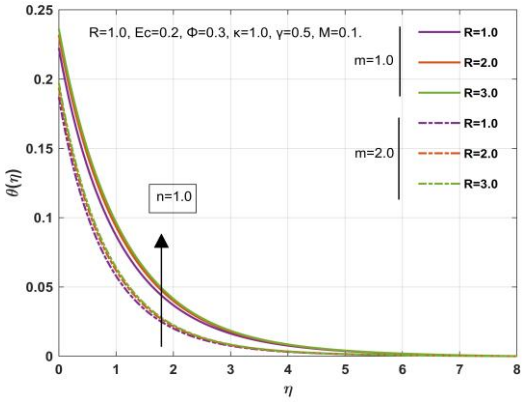

(b) Radiation effect on Newtonian fluid

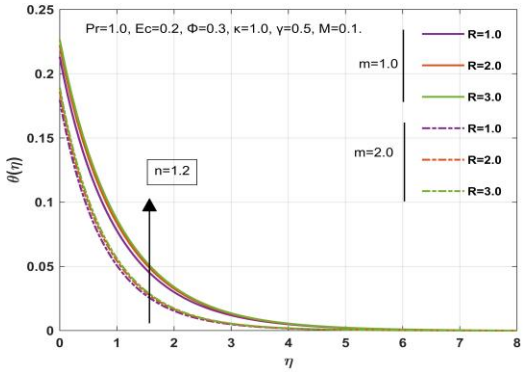

(c) Radiation effect on Dilatant Fluid

Figure 7: (a-c) Diversity of *R* parameter on thermal transport

5.1 Tabulated Analysis

Tables 3 and 4 present the variations in skin-friction coefficient and Nusselt number, respectively, for different values of the magnetic parameter M, curvature parameter κ, Prandtl number Pr, Eckert number Ec, and radiation parameter R under both linear ($m = 1$) and nonlinear ($m = 2$) stretching conditions. The results are reported for pseudoplastic ($n = 0.8$), Newtonian ($n = 1.0$), and dilatant ($n = 1.2$) fluids.

The analysis reveals a consistent influence of stretching nonlinearity on both skin friction and heat transfer. In all cases, nonlinear stretching ($m = 2$) produces higher skin-friction coefficients and higher Nusselt numbers compared with linear stretching ($m = 1$).

Table 3: Evaluation of Skin Friction

M	κ	m=1			m=2		
		n=0.8	n=1.0	n=1.2	n=0.8	n=1.0	n=1.2
0.1	1.0	0.7875	0.7642	0.7594	0.8639	0.8419	0.8373
0.3		0.8303	0.8038	0.7964	0.8962	0.8703	0.8627
0.5		0.8677	0.8381	0.8280	0.9254	0.8959	0.8853
0.1	1.0	0.7875	0.7642	0.7594	0.8639	0.8419	0.8373
	2.0	0.9457	0.8808	0.8498	1.0001	0.9395	0.9112
	3.0	1.0735	0.9759	0.9244	1.1131	1.0207	0.9731

Table 4: Evaluation of Nusselt Number

Φ	M	Pr	Ec	κ	R	m=1			m=2		
						n=0.8	n=1.0	n=1.2	n=0.8	n=1.0	n=1.2
0.3	0.1	1.0	0.2	1.0	1.0	0.4818	0.4989	0.5099	0.4976	0.5174	0.5293
0.6						0.7742	0.8100	0.8334	0.8085	0.8524	0.8795
0.9						0.9704	1.0224	1.0568	1.0211	1.0868	1.1283
0.3	0.1					0.4818	0.4989	0.5099	0.4976	0.5174	0.5293
	0.3					0.4728	0.4894	0.5002	0.4906	0.5105	0.5226
	0.5					0.4651	0.4813	0.4919	0.4844	0.5044	0.5167
	0.1	1.0				0.4818	0.4989	0.5099	0.4976	0.5174	0.5293
		2.0				0.4928	0.5129	0.5258	0.5109	0.5332	0.5464
		3.0				0.4950	0.5173	0.5314	0.5146	0.5388	0.5529
		1.0	0.2			0.4818	0.4989	0.5099	0.4976	0.5174	0.5293
			0.4			0.4349	0.4603	0.4766	0.4571	0.4848	0.5012
			0.6			0.3881	0.4217	0.4432	0.4166	0.4522	0.4731
			0.2	1.0		0.4818	0.4989	0.5099	0.4976	0.5174	0.5293
				2.0		0.5047	0.5227	0.5350	0.5213	0.5415	0.5540
				3.0		0.5170	0.5346	0.5472	0.5337	0.5536	0.5665
				1.0	1.0	0.4818	0.4989	0.5099	0.4976	0.5174	0.5293
					2.0	0.7382	0.7670	0.7854	0.7648	0.7982	0.8182
					3.0	0.9940	1.0345	1.0604	1.0315	1.0786	1.1068

This behavior indicates that an increase in the stretching intensity enhances both the velocity and temperature gradients at the cylinder surface, thereby augmenting the rates of momentum and heat transfer. As presented in Table 3, the skin friction coefficient $-h''(0)$ is larger for $m = 2$ compared to $m = 1$, signifying steeper velocity gradients and, consequently, a thinner momentum boundary layer. This facilitates more efficient convective heat transport away from the surface, which accounts for the lower temperatures observed for $m = 2$ in Figure 2.

Transitions in values of parameters display the expected trends. An increase in the magnetic parameter decreases both skin friction and Nusselt number due to the opposing Lorentz force. On the other hand, a higher curvature parameter intensifies both quantities by strengthening the geometric stretching effect. In the case of heat transfer, a higher Prandtl number and radiation parameter enhance the Nusselt number, whereas larger Eckert number reduces it due to viscous dissipation. While the magnitude of these effects fluctuates among the three fluid types, the influence of nonlinear stretching remains dominant, consistently improving momentum and thermal transport across all parameters.
Overall, the results demonstrate that nonlinear stretching significantly enhances the wall shear stress and heat-transfer performance for pseudoplastic, Newtonian, and dilatant fluids, and the observed trends are robust across the entire parametric range considered in the study.

6 Conclusion

The thermal transport of power-law fluid across a non-linearly stretched cylinder is examined computationally. To convert the system of BVPs, the governing PDEs are changed into ODEs using a similarity transformation. BVP4C is subsequently utilised for numerical solutions. The thermal transport characteristics were analysed using several governing parameters, including the n, magnetic variable M, velocity exponent m, Prandtl parameter Pr, and surface convection κ. The numerical finding for skin friction is consistent with previous investigations. Numerical results for the $h''(0)$, and $\theta'(0)$ are computed. Graphs displaying the temperature profiles are presented for various combinations of relevant parameter. The obtained results lead to the following deductions

- The study demonstrates that stretching nonlinearity plays a dominant role in heat and momentum transport. Nonlinear stretching (m=2) consistently produces higher skin-friction coefficients and larger Nusselt numbers than linear stretching (m=1), confirming that stronger stretching intensifies both velocity and thermal gradients at the wall.

- Thermal profiles engage differently for linear and nonlinear stretching, depending on the controlling parameter. For Ec, M, κ, ϕ, and R, linear stretching leads to higher temperature distributions due to stronger and more uniform shear. Conversely, for the Prandtl number, nonlinear stretching exhibits a stronger temperature reduction because the weakened shear environment allows thermal diffusivity effects to dominate.

- All heat-generating mechanisms *i.e.,* viscous dissipation, magnetic damping, surface convection, and radiation intensifies the temperature field, but their influence differs by rheology. Pseudoplastic

fluids show steeper thermal responses due to shear-thinning; Newtonian fluids exhibit moderate behaviour, while dilatant fluids maintain more thermal resistance because of shear-thickening effects.

- Geometric stretching through curvature (κ) effectively enhances heat removal, thinning the thermal boundary layer across all fluids. This geometric effect aligns with the table-based observation that curvature intensifies both skin friction and Nusselt numbers, confirming its stabilizing influence on convective transport.

- Magnetic parameter M consistently suppresses velocity and heat transfer, reflected by reducing Nusselt numbers and skin friction in Tables 3–4. This aligns with the graphical rise in temperature under stronger Lorentz force, as magnetic damping reduces convective heat loss.

- Prandtl number Pr strengthens heat-transfer performance, increasing the Nusselt number while decreasing the temperature profile. This dual behaviour develops the classical thermal diffusivity mechanism and confirms the opposite, but complementary behaviour observed in the temperature graphs.

7 Future Work

Future research may extend this study by including more complex rheological models such as Carreau, Cross, or Sisko fluids to capture broader shear-dependent behaviours. Time dependent stretching or oscillatory motion could further clarify unsteady thermal momentum interactions, while variable thermal conductivity or temperature-dependent viscosity would increase realism in high-temperature processes. Inclusion of nanoparticle suspensions, chemical reactions, or entropy generation analysis may also deepen understanding of thermal efficiency. Finally, validating the present computational trends through experimental or high-resolution numerical simulations would strengthen the applicability of these findings to engineering systems involving curved geometries and non-Newtonian materials.

References

[1] Usman, P. Lin, and A. Ghaffari, “Steady flow and heat transfer of the power-law fluid between two stretchable rotating disks with non-uniform heat source/sink: Usman et al.,” *Journal of Thermal Analysis and Calorimetry*, vol. 146, no. 4, pp. 1735–1749, 2021.

[2] Y. Zhang, Y. Zhang, Y. Bai, B. Yuan, and L. Zheng, “Flow and heat transfer analysis of a maxwell-power-law fluid film with forced thermal marangoni convective,” *International Communications in Heat and Mass Transfer*, vol. 121, p. 105062, 2021.

[3] A. Srivastav and C. RamReddy, “Numerical estimations in a power-law fluid flow with thermal radiation: a complete case study,” *Radiation Effects and Defects in Solids*, vol. 178, no. 3-4, pp. 429–441, 2023.

[4] A. K. Pandey, K. Bhattacharyya, A. K. Gautam, S. Rajput, M. S. Mandal, A. J. Chamkha, and D. Yadav, “Insight into the relationship between non-linear mixed convection and thermal radiation: The

case of newtonian fluid flow due to non-linear stretching," *Propulsion and Power Research*, vol. 12, no. 1, pp. 153–165, 2023.

[5] A. Ghaffari, I. Mustafa, T. Muhammad, Y. Altaf, *et al.*, "Analysis of entropy generation in a power-law nanofluid flow over a stretchable rotatory porous disk," *Case Studies in Thermal Engineering*, vol. 28, p. 101370, 2021.

[6] Z. Elahi, M. Khalid, and A. Shahzad, "Analysis of heat transfer of power-law fluid along a vertical stretching cylinder," *Innovative Journal of Mathematics (IJM)*, vol. 1, no. 3, pp. 1–11, 2022.

[7] J. Ahmed, M. Khan, Z. Rasheed, A. Ahmed, L. Ahmed, and A. Bhandari, "Entropy generation analysis for axisymmetric flow of carreau nanofluid over a horizontally stretching cylinder," *Proceedings of the Institution of Mechanical Engineers, Part E: Journal of Process Mechanical Engineering*, vol. 236, no. 6, pp. 2283–2295, 2022.

[8] A. Shahzad, Z. Shamim, and T. Naseem, "Flow and heat transfer of power law fluid over horizontal stretching cylinder with partial slip condition and thermal radiation," 2022.

[9] A. M. Sedki, "Effect of thermal radiation and chemical reaction on mhd mixed convective heat and mass transfer in nanofluid flow due to nonlinear stretching surface through porous medium," *Results in Materials*, vol. 16, p. 100334, 2022.

[10] T. Salahuddin, M. Awais, and W.-F. Xia, "Variable thermo-physical characteristics of carreau fluid flow by means of stretchable paraboloid surface with activation energy and heat generation," *Case Studies in Thermal Engineering*, vol. 25, p. 100971, 2021.

[11] B. Xie and Y.-M. Wang, "Stagnation-point flow and heat transfer of power-law mhd fluid over a stretching surface with convective heat transferboundary condition," *International Journal of Numerical Methods for Heat & Fluid Flow*, vol. 32, no. 1, pp. 265– 282, 2022.

[12] M. Ferdows, M. Shamshuddin, S. Salawu, and S. Sun, "Thermal cooling performance of convective non-newtonian nanofluid flowing with variant power-index across moving extending surface," *Scientific reports*, vol. 12, no. 1, p. 8714, 2022.

[13] R. P. Sharma and S. Shaw, "Mhd non-newtonian fluid flow past a stretching sheet under the influence of non-linear radiation and viscous dissipation," *Journal of Applied and Computational Mechanics*, vol. 8, no. 3, pp. 949–961, 2022.

[14] A. Raptis, "Radiation and viscoelastic flow," *International Communications in Heat and Mass Transfer*, vol. 26, no. 6, pp. 889–895, 1999.

[15] J. Ahmed, S. Bourazza, M. Sarfraz, M. Orsud, S. M. Eldin, N. A. Askar, and M. A. Elkotb, "Heat transfer in jeffrey fluid flow over a power law lubricated surface inspired by solar radiations and magnetic flux," *Case Studies in Thermal Engineering*, vol. 49, p. 103220, 2023.

[16] N. Hameed, S. Noeiaghdam, W. Khan, B. Pimpunchat, U. Fernandez-Gamiz, M. S. Khan, and A. Rehman, "Analytical analysis of the magnetic field, heat generation and absorption, viscous

dissipation on couple stress casson hybrid nano fluid over a nonlinear stretching surface," *Results in Engineering*, vol. 16, p. 100601, 2022.

[17] H. Ullah, T. Hayat, S. Ahmad, and M. S. Alhodaly, "Entropy generation and heat transfer analysis in power-law fluid flow: Finite difference method," *International Communications in Heat and Mass Transfer*, vol. 122, p. 105111, 2021.

[18] A. Aziz, "A similarity solution for laminar thermal boundary layer over a flat plate with a convective surface boundary condition," *Communications in Nonlinear Science and Numerical Simulation*, vol. 14, no. 4, pp. 1064–1068, 2009.

[19] A. Ishak, "Similarity solutions for flow and heat transfer over a permeable surface with convective boundary condition," *Applied Mathematics and Computation*, vol. 217, no. 2, pp. 837–842, 2010.

[20] S. R. Mishra, S. Baag, G. C. Dash, and M. R. Acharya, "Numerical approach to mhd flow of power-law fluid on a stretching sheet with non-uniform heat source," *Nonlinear Engineering*, vol. 9, no. 1, pp. 81–93, 2019.

[21] M. S. Abel, J. Tawade, and M. M. Nandeppanavar, "Effect of non-uniform heat source on mhd heat transfer in a liquid film over an unsteady stretching sheet," *International Journal of Non-Linear Mechanics*, vol. 44, no. 9, pp. 990–998, 2009.

[22] H. Andersson, "Film flow of power-law fluids," *Encyclopedia of Fluid Mechanics*, vol. 9, pp. 617–648, 1990.